Effects of Wall Cooling on Supersonic Modes in High-Enthalpy Hypersonic Boundary Layers over a Cone

Chau-Lyan Chang[1]
NASA Langley Research Center, Hampton, VA 23681

Heather Kline[2]
National Institute of Aerospace, Hampton, VA 23666

and

Fei Li[3]
NASA Langley Research Center, Hampton, VA 23681

High-enthalpy hypersonic boundary-layer transition plays an important role in many entry/descent vehicles. Aerothermodynamic performance of these vehicles strongly depends on the transition location on the surface. However, detailed transition flow physics in these chemically reacting boundary layers are poorly understood and transition estimates during the design phase rely heavily on empirically-derived transition criteria such as Re_θ/M_e. One of the most intriguing characteristics in hypersonic boundary layers is the presence of *unstable* supersonic modes, first identified in the 1990s. Due to a recent surge in hypersonic applications, there has been renewed interest in studying the flow physics of supersonic modes using either theory or direct numerical simulations. This paper investigates the rise of supersonic modes in a high-enthalpy hypersonic flow over a 5° half-angle cone at various wall temperatures using both quasiparallel linear stability theory and linear PSE. It was found that supersonic modes exist in all wall temperature conditions including the adiabatic wall case. Cooler wall temperature causes the second Mack mode to become an unstable supersonic mode naturally downstream of the upper-branch neutral location when the wall is sufficiently cooled. In terms of the integrated growth, the second mode is still the dominant mode. Nonetheless, supersonic modes can cause additional series of relatively weaker growth than that of the second mode beyond the peak amplitude location. According to the present linear PSE results, contrary to what was speculated in the literature, supersonic-mode pressure disturbance structure radiated into the freestream is nonacoustic in nature and the formation of unstable supersonic modes is mainly associated with the synchronization of phase speed between the instability and acoustic waves in a nonparallel boundary layer, not due to nonlinear modal interaction as suggested in the literature.

Nomenclature

C = species concentration
c_r = phase speed of the disturbance
f = disturbance frequency (Hz)
G = normalized generalized inflectional quantity ($\frac{d}{dy}\left(\rho\frac{du}{dy}\right)$)
i = imaginary constant
l = boundary-layer similarity length scale ($=\sqrt{\nu_e x/U_e}$)
M = freestream Mach number
M_e = boundary edge Mach number

[1] Aerospace Technologist, Computational AeroSciences Branch, Email: Chau-Lyan.Chang@nasa.gov, Associate Fellow, AIAA.
[2] Research Engineer, Research Department, Member, AIAA
[3] Aerospace Technologist, Computational AeroSciences Branch.

p_r = real part of the linear pressure perturbation
Re_x = length Reynolds number
Re_θ = momentum thickness Reynolds number
R = Reynolds number based on boundary-layer similarity length scale ($= U_e l/\nu_e = \sqrt{Re_x}$)
T_w = wall temperature
u = streamwise velocity
U_e = boundary-layer edge velocity
x = streamwise coordinate
y = wall-normal coordinate
α = streamwise wave number
ϕ = arbitrary disturbance quantity
ρ = density
ν_e = boundary-layer edge kinematic viscosity

I. Introduction

Hypersonic transition research in the past few decades has advanced substantially due to the availability of supersonic quiet tunnels and large-scale computational facilities [1-2]. Various instability wave mechanisms across the speed regimes have been studied extensively via higher fidelity methods such as linear/nonlinear parabolized stability equations (PSE) or direct numerical simulations (DNS). In many cases, cross validations of computations and experimental measurements led to much better understanding of the intricate transition flow physics (e.g., [3-4]). For hypersonic boundary layers with calorically perfect gases, the second Mack mode [5] has been pursued in earnest both experimentally and computationally for various Mach numbers in recent years (e.g., [6-7]). In contrast, instability mechanisms for high-enthalpy, chemically reacting boundary layers at even higher Mach numbers have received relatively little attention in the same period. Nonetheless, for entry/descent hypersonic applications, understanding and further predicting transition beyond the commonly used Re_θ/M_e criterion plays a crucial role in the success or failure of future hypersonic vehicles.

For hypersonic boundary layers, second and ever higher modes can become unstable with the second mode being the dominant disturbances for slender configurations lacking the crossflow instability. For low-enthalpy, nonreacting hypersonic boundary layers, the linear/nonlinear evolution until early breakdown stage for second modes is relatively well understood both from theoretical/computational and experimental perspectives. Unfortunately, its high-enthalpy counterpart remains poorly understood due to limited research activities. Effects of reacting flow chemistry on boundary-layer stability have been investigated somewhat actively during the 1990s and early 2000s (for example, [8-11]). It was found that reacting flow chemistry plays an important role in transition. For high-enthalpy flat plate boundary layers, transition onset moves upstream substantially if the finite-rate chemistry effect is fully accounted for [8-9]. Very interestingly, in Ref. [8], unstable supersonic modes were identified downstream of the peak second-mode growth rate location for both reacting and nonreacting boundary layers with a boundary-layer edge Mach number of around 12.5. Supersonic modes, by definition, travel with a phase speed that is larger than the speed of sound relative to the freestream. Their phase speeds are smaller than that of the corresponding upstream propagating acoustic waves. Supersonic modes exist in supersonic boundary layers but with usually a very stable growth rate. For this reason, supersonic modes were rarely identified in stability calculations nor did they play any role in supersonic boundary-layer transition. During the recent resurgence in hypersonic transition research, other researchers have also found unstable supersonic modes in reacting boundary layers with either thermal equilibrium or nonequilibrium (e.g., [12-14]). From DNS simulation results, these unstable supersonic modes were also found to be present downstream of the peak second-mode location and they may have relatively large growth rate spikes under either a cold or hot wall condition. It remains unknown if wall temperature plays a significant role in the rise of supersonic modes. In Ref. [14], it was also found that quasiparallel linear stability theory (LST) fails to capture supersonic modes and unstable and relatively large growth rate supersonic modes are only present in DNS results. They also attribute the onset of significant supersonic-mode growth to nonlinear interaction of unstable subsonic mode, stable supersonic mode, and the slow acoustic spectrum.

Despite recent confirmation of the existence of unstable supersonic modes in reacting hypersonic boundary layers, the flow physics of supersonic modes remain poorly understood. Many issues related to this intriguing phenomenon need to be sorted out in future research. For instance, the onset of unstable supersonic modes and its relation with respect to boundary-layer edge Mach number remains an open question. In addition, the relation of wall cooling with

the onset of unstable supersonic modes and the effects that thermochemical nonequilibrium has on them remain largely unknown. DNS is not the right tool for a comprehensive study to answer these questions due to its high cost. A more logical choice is to use a PSE solver for a more comprehensive parametric study concerning all the issues alluded to above. Linear PSE has been used in Ref. [8] to identify unstable supersonic modes. Combining with the fact that LST cannot capture supersonic modes (as concluded in [14]), it is reasonable to assume that nonparallel effects need to be accounted for in capturing the onset of supersonic modes. This paper is intended to address the above issues and hypothesis by employing a combination of LST and PSE solvers. To facilitate parametric studies, a finite-rate reacting flow boundary-layer code, in addition to the usual CFD solvers, is used to generate mean flows with different freestream conditions. A canonical hypersonic flow around Mach 10 over a 5° half-angle cone is chosen for the parametric study. In the following sections, a brief discussion of the mean flow and stability solutions is given, followed by a detailed description of the current stability results. A brief summary of the findings is given at the end.

II. Stability and Mean Flow Computations

Flow instability computations for reacting hypersonic boundary layers in this paper are carried out by using the NASA in-house LAngley Stability and TRansition Analysis Code (LASTRAC) version 3.0 [15-16]. This new version extends the widely used LASTRAC software [17] for chemically reacting hypersonic boundary layers by accounting for full chemistry effects due to multicomponents gases. Both thermal equilibrium and nonequilibrium effects are handled by user-supplied chemistry models. These models can be provided by users using either dynamically linked shared libraries written in a set of prototyped C++ functions or an ASCII table. A default built-in five species chemistry model is also available without any user input. This new version is implemented within the framework of existing modules using the object-oriented paradigm. The design of the software ensures backward compatibility, ease of user-provided mean flow interfaces, independence of a chemistry model from the solver, and flexible chemistry models and properties input. Users provide the reacting mean flow via additional input profiles and run the code in the same way as the old perfect gas version. Similar to the old version, both global eigenvalue spectra and local eigenvalue refinement using Newton's method are available for unstable mode search. The matrix size for reacting flows is dependent on how many species and thermal equilibrium conditions are required in the chemistry model. In general, an eigenvalue search would be more time consuming for reacting flows. The current version only works for 2D/axisymmetric/infinite-swept-wing chemically reacting boundary layers for LST and linear PSE solutions. Extension to full 3D boundary layer and nonlinear PSE is under development, with both capabilities only available for a perfect gas at present.

A mean flow solution is required as an input to the LASTRAC code, in a body-fitted format with flow profiles on lines normal to the surface. The legacy reacting flow boundary-layer code written by Blottner [18] was used to generate mean flow solutions for a hypersonic flow over a sharp-tip 5° half-angle cone with finite-rate but thermally equilibrium chemistry. The code allows wall boundary conditions to be changed from adiabatic to any specified wall temperature. The legacy Fortran code was modified to compute the wall-normal velocity component needed for linear PSE computations and to output Fortran unformatted mean flow file format to interface with LASTRAC.

Mean flow solutions with thermochemical nonequilibrium use VULCAN [19, 20], which employs Arrhenius reaction rates and Millikan-White relaxation time equations. CFD meshes were generated using Pointwise®. To avoid numerical issues around the sharp tip of the cone, a small nose radius of 1 mm is added to the cone. The mesh for this axisymmetric cone simulation uses 993 points in the streamwise direction and 589 points in the normal direction, with closer spacing near the nose with an excess of 100 points in the streamwise direction on the blunt nose. These dimensions were chosen in order to provide a sufficient number of points to refine the nose of the cone as well as the boundary layer and shock. The mesh refinement capabilities of VULCAN were used for shock capturing. Wall boundary conditions are no-slip and isothermal, with a symmetry boundary condition along the axis of rotation. The gas is 5-species air (O2, N2, N, O, and NO) using either Dunn & Kang [21] as reviewed by Gupta et al. [22] and Blottner [23], or Park reaction rate coefficients [24]. The reaction rates used for each flow solution is noted for each case, and is used for both the mean flow calculations as well as the stability analysis.

III. Results

One of the main goals of this research is to understand the onset of unstable supersonic modes in high-enthalpy boundary layers, even though this phenomenon could happen for calorically perfect gas as well (see [8]). A canonical boundary layer for a hypersonic flow with varying Mach numbers over a sharp-tip 5° half-angle cone is chosen for

the study. Blottner's boundary-layer code [18] is used to generate finite-rate reacting boundary-layer mean flows in thermal equilibrium. Five species (O_2, N_2, O, N, NO), 8 reactants (3 catalytic bodies), and 6-reaction chemistry models are used for both mean flow and stability computations [8, 23]. As mentioned above, for thermochemical nonequilibrium boundary layers with the same number of species and reactions, the VULCAN code [19, 20] is used.

A. Onset of Unstable Supersonic Modes in Thermochemical Equilibrium with Significant Chemical Reaction

While unstable supersonic modes have been identified numerically for hypersonic flows with or without chemical reactions, it was found in Ref. [8] that chemical reactions enhance supersonic modes for several canonical configurations at a Mach number around 12. The first set of computations is focused on investigating the onset of unstable supersonic modes for a hypersonic boundary layer past a 5° half-angle cone with significant chemical reactions under thermal equilibrium. The assumption of thermal equilibrium is to allow the use of Blottner's boundary-layer code [18] for parametric studies. Effects of thermochemical nonequilibrium will be discussed later in this section. The post-shock (boundary-layer edge) Mach number, temperature, and unit Reynolds number are set to be 9.03, 1282.9 K, and $3.26 \times 10^6\ /m$, respectively, in the boundary-layer mean flow calculations. The corresponding preshock freestream Mach number is about 10.4 and a static temperature of about 1050 K for the cone configuration. Adiabatic wall and wall temperatures of 1000 K and 500 K in thermal equilibrium are investigated for comparison.

Figure 1(a) shows the temperature and streamwise velocity variation along the wall-normal distance for three wall conditions at a boundary-layer scale Reynolds number of $R = 2000$. Under the cooled wall conditions, the peak temperature inside the boundary layer drops to only about 3.2 times the edge temperature, even though substantial extent of chemical reactions could still take place around the peak temperature regions, as is evident from the species N_2 and NO distribution shown in Figs. 1(b) and 1(c), respectively. Figure 1(d) shows the corresponding streamwise velocity and generalized inflectional quantity ($G = \frac{d}{dy}\left(\rho \frac{du}{dy}\right)$) near the critical region where this quantity is zero (generalized inflectional point). The streamwise velocity at the outer (away from wall) generalized inflection (critical) point is about 0.94, 0.87, and 0.84, for an adiabatic wall, $T_w = 1000\ K$, and $T_w = 500\ K$, respectively. This implies that as the wall temperature is reduced, the boundary layer becomes thinner and the outer generalized inflectional point moves toward the wall to a location with a smaller convecting speed. Subsonic modes under this condition have a phase speed of $c_r > 1 - \frac{1}{M_e} = 0.889$. The critical points for two wall cooling cases have a convecting speed that is smaller than the threshold phase speed at this given Mach number. As we will see later, this results in the emergence of unstable supersonic modes.

Instability modes at the above streamwise location can be visualized by performing a frequency scan using LST. Results shown in Fig. 2 reveal the presence of both second- (first hump) and third-mode (second hump) instability waves, typical for a hypersonic boundary layer at this Mach number. All instability modes captured belong to a subsonic mode as is evident from Fig. 2(b). At this location, third mode disturbances appear to be stable for all three wall temperatures.

Based on the above results, instability evolution along the streamwise direction is studied for a chosen frequency at each wall condition ($250\ kHz$ for adiabatic wall and $500 kHz$ for two wall-cooling cases). Results for adiabatic and the colder wall case ($T_w = 500\ K$) are discussed in more detail in the context of the onset of supersonic modes below. Figure 3 depicts growth rates versus streamwise distance for the adiabatic wall case with $f = 250\ kHz$. This second mode results in an N factor of about 8 from linear PSE. Apparently, both LST and PSE predict the mode to be subsonic throughout the domain. The phase speed ranges from 0.92 to 0.96, quite typical of second mode disturbances at high Mach numbers. Hereafter, the phase speed for linear PSE is computed by normalization with the total kinetic energy, unless otherwise noted. It is an averaged value since the phase speed in a nonparallel boundary layer varies along the wall-normal direction and with different flow variables. Similarly, nonparallel growth rates from all linear PSE computations are based on the total kinetic energy unless otherwise noted. One interesting question to ask is: does supersonic mode exist under this condition? The answer is yes from the results shown in Fig. 4 where the LST-predicted subsonic mode (as the one shown in Fig. 3) is plotted along with a much more stable supersonic mode along the streamwise direction. These two (supersonic and subsonic) branches of discrete instability modes are closely associated with what is often referred to in the literature as the fast (F) and slow acoustic (S) modes with a phase speed less than $1 + \frac{1}{M_e}$ and greater than $1 - \frac{1}{M_e}$, respectively. Hereafter, these two branches are referred to as the subsonic (S mode) and supersonic (F mode) modes from instability wave standpoint, even though the phase speed of the supersonic (F) mode branch becomes subsonic sufficiently upstream (e.g., for $x < 1.6\ m$ in Fig. 4). Near $x = 1\ m$,

the LST computations lost track of the supersonic mode and locks on to the subsonic mode for $x < 1\ m$. Two branches of instability modes cross each other with the same phase speed at around $x = 1.27\ m$. This location, usually referred to as the synchronous point of the fast and slow modes, is well before the second mode peak and the supersonic mode is highly damped. This explains why no unstable supersonic mode is present in Fig. 3 as that would happen at lower wall temperature to be discussed below.

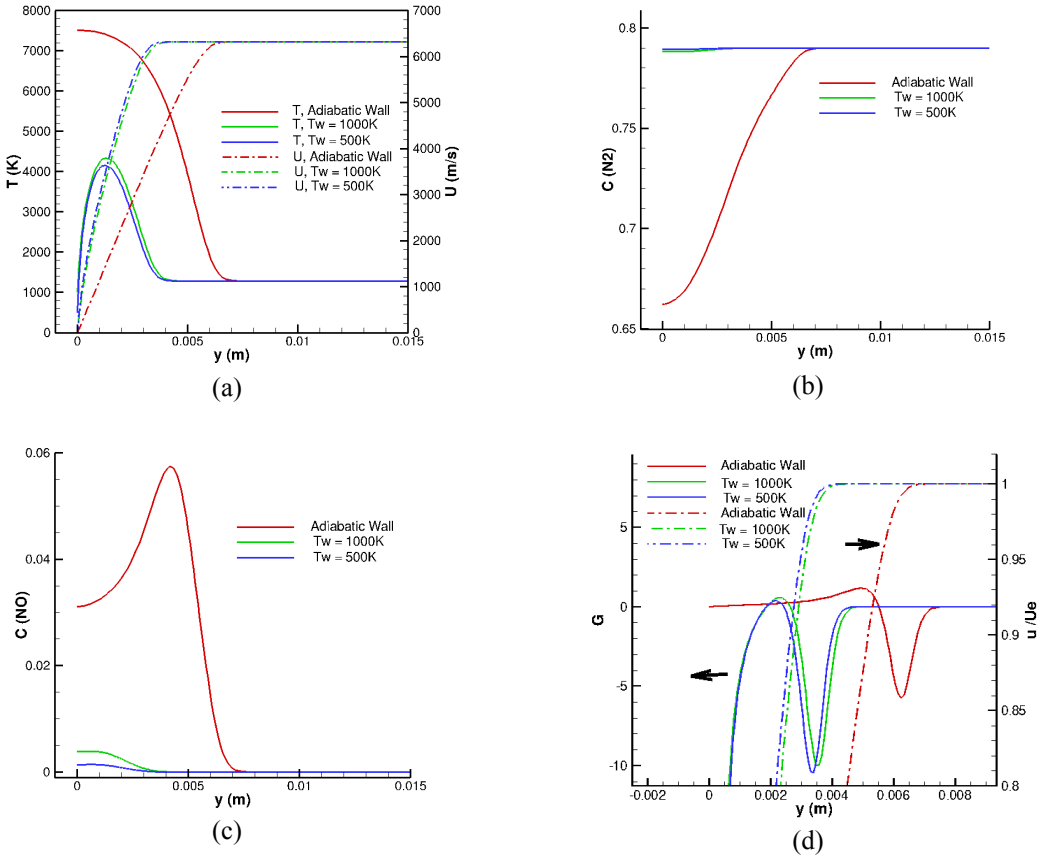

Figure 1. Blottner's boundary-layer code predicted mean profiles at $R = 2000$ under three different wall temperatures: (a) temperature and velocity distribution, (b) concentration of species N_2, (c) concentration of species NO, and (d) generalized inflectional quantity and streamwise velocity.

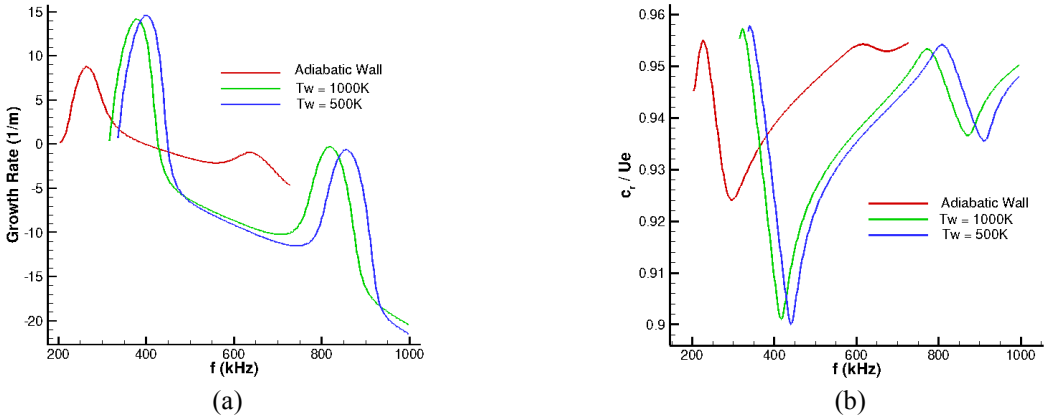

Figure 2. Disturbance growth rates and phase speed versus frequency at $R = 2000$ under three different wall temperatures: (a) dimensional growth rate and (b) nondimensional phase speed normalized by edge velocity.

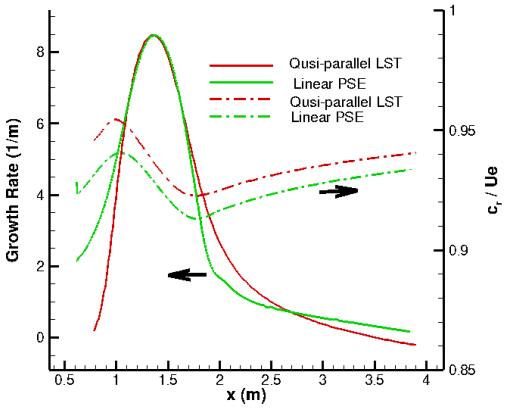

Figure 3. Disturbance growth rate and phase speed along the streamwise direction for $f = 250kHz$ under adiabatic wall condition predicted by LST and linear PSE (measured by total kinetic energy).

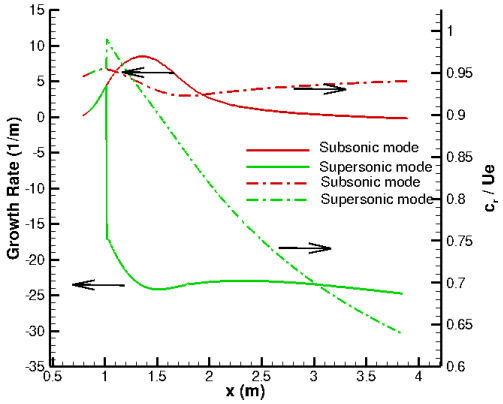

Figure 4. Subsonic and supersonic modes for $f = 250kHz$ under adiabatic wall condition along the streamwise direction predicted by quasiparallel LST.

To understand how supersonic modes evolve beyond the second mode peak (near minimum phase speed around $x = 1.8\,m$, where the onset usually takes place according to previous studies), two more PSE computations were carried out by initiating the disturbances with either a subsonic or supersonic mode. The initial conditions were obtained by the approximated nonparallel eigenmode calculations described in the LASTRAC manual [17]. Interestingly, results shown in Fig. 5 reveal that if a subsonic mode is initiated at this location, the PSE solution tracks the same solution obtained by initializations at a much further upstream location as shown in Fig. 3, without any noticeable transient effects. On the other hand, if a supersonic mode is manually excited (here, the term manual excitation means that a supersonic mode obtained from a nonparallel eigenmode is manually added at $x = 1.8\,m$ in the linear PSE or DNS computations, in addition to the regular mode that initiates further upstream; in other words, the supersonic mode does not rise automatically as a continuation of second mode disturbances), both growth rate and phase speed show some transient supersonic behavior before the disturbance eventually locks on to the regular subsonic modes. The spiky growth rates oscillate between positive and negative values with a short scale, reminiscent of what is observed in unstable supersonic modes captured in DNS under similar conditions [14]. The results also resemble those for the cold wall case shown in Fig. 6 (a) where disturbance evolution along the streamwise direction is depicted for a disturbance frequency of 500 kHz for the cold wall case of $T_w = 500\,K$. In this latter case, though, unstable supersonic modes predicted by linear PSE automatically rise near the upper branch neutral location of the second mode without the need of manual excitation, as was done for the adiabatic wall case above. The LST results for the same case, in contrast, are entirely subsonic. The linear PSE predicted phase speed also undergoes small-scale oscillations before it eventually settles down to an almost constant value of 0.86. Figure 6 (a) also shows that the supersonic mode eventually becomes a neutral mode with a constant phase speed and an almost constant growth rate. Despite the seemingly large alternating growth rate after the onset of unstable supersonic mode shown in this case, the integrated N factor shown in Fig. 6 (b) exhibits mild departure from the LST predicted disturbance growth. The alternating grow and decay of supersonic modes prevents significant disturbance growth from happening. Grid convergence results are shown for this case in Fig. 6 (c) with four different streamwise step sizes ranging from 2 mm to 0.25 mm. The wall normal grid has a constant increment of $y/l = 0.5$ beyond the stretched mesh near the critical layer (see p. 22 in Ref. [17]) with a total of 481 points. As can be seen, linear PSE solutions collapse for all four step sizes both in the second-mode region and the first three growth rate spikes. Small differences still exist for the less important small spikes and neutral regions. For all PSE computations shown hereafter, a streamwise step size of 1 mm is used.

The linear stability theory predicted eigenmodes for this cold wall case at $500kHz$ are shown in Fig. 7. In addition to the unstable subsonic modes, there also exists a stable supersonic mode. The synchronous point where two modes have the same phase speed (of 0.91) occurs at $x = 0.83\,m$, slightly downstream of the peak second mode location. Due to nonparallel effects, the true synchronous location should be slightly further downstream, as will be discussed further below. In this vicinity, disturbances would have reached a relatively large amplitude due to the substantial second-mode growth (an integrated N factor of about 5). This proximity of phase speed between the subsonic second

and supersonic modes apparently triggers the spontaneous growth of supersonic modes as shown in Fig. 6. Numerical experiments similar to that shown in Fig. 5 were also carried out around $x = 1.05\,m$, slightly downstream of the synchronous point. From the local nonparallel eigenmode spectra, one subsonic and two supersonic modes were identified. Linear PSE results using these three initial modes are compared with the regular solution (as shown in Fig. 6) in Fig. 8. Again, the subsonic mode initialization closely follows that of the regular solution except for some minor transient effects. On the contrary, both supersonic modes initializations track pure supersonic phase speeds (lower than 0.89) throughout the domain. One of the two modes is more unstable. The regular mode shown in Fig. 6 is basically tracking the more unstable nonparallel supersonic mode in terms of growth rate for $x > 1.1\,m$. These results reveal that under the cold wall condition, supersonic modes emerge naturally downstream of the peak second mode location. The growth rate exhibits a positive to negative oscillation around one of the nonparallel supersonic eigenmodes but with a phase speed that is also oscillatory but with a mean value closer to the subsonic mode. The mixed supersonic and subsonic behavior of the unstable supersonic modes shown here is a direct outcome of mode transition slightly downstream of the synchronous location between the subsonic and supersonic branches. It is evident that the rise of supersonic modes is significantly enhanced by wall cooling. The onset of supersonic modes does not take place automatically under adiabatic wall conditions as seen above.

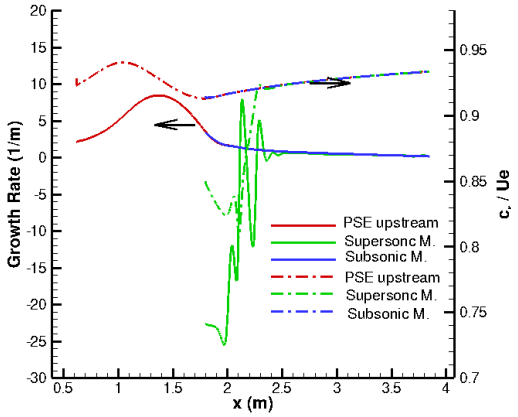

Figure 5. Linear PSE computed disturbance growth rate and phase speed for $f = 250\,kHz$ under adiabatic wall condition via three different initial starting conditions.

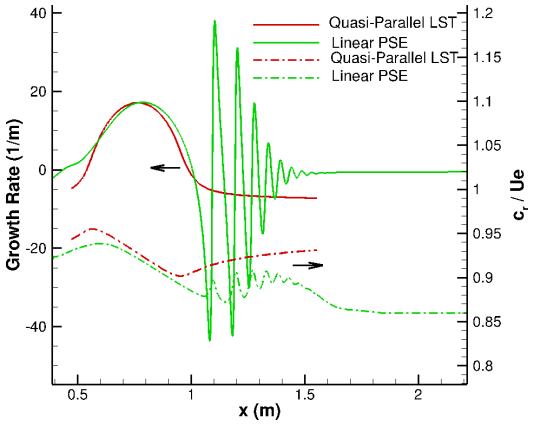

(a)

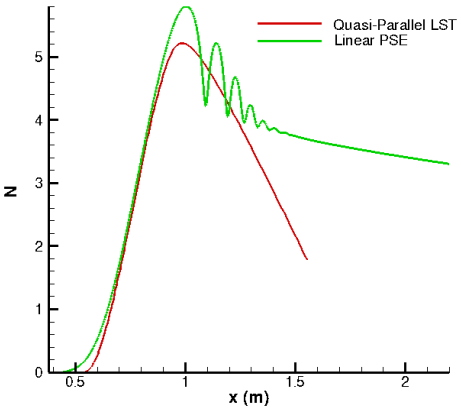

(b)

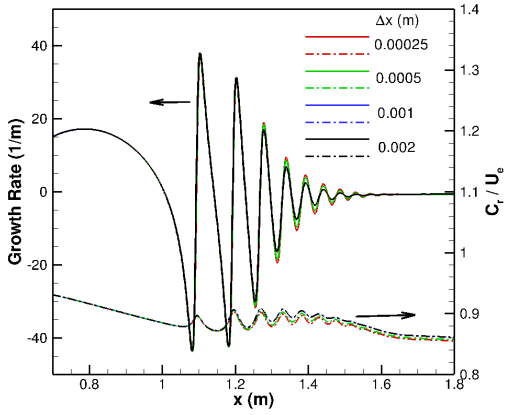

(c)

Figure 6. Disturbance growth rate, phase speed and N factor along the streamwise direction for $f = 500\,kHz$ under $T_w = 500\,K$, predicted by LST and linear PSE: (a) growth rates and phase speed from LST and PSE, (b) N factor predicted by LST and PSE, and (c) grid convergence for linear PSE with various streamwise step sizes.

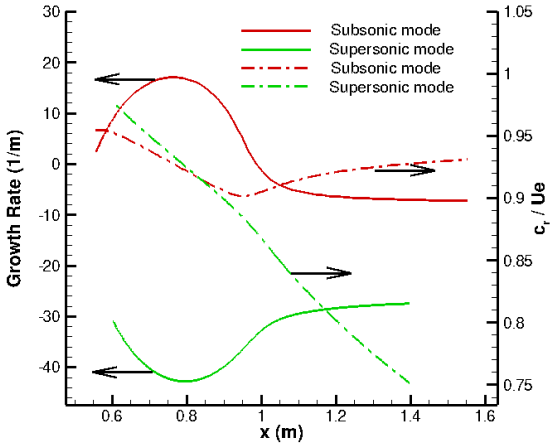

Figure 7. Subsonic and supersonic modes for $f = 500kHz$ under cold wall condition ($T_w = 500\ K$) along the streamwise direction predicted by quasiparallel LST.

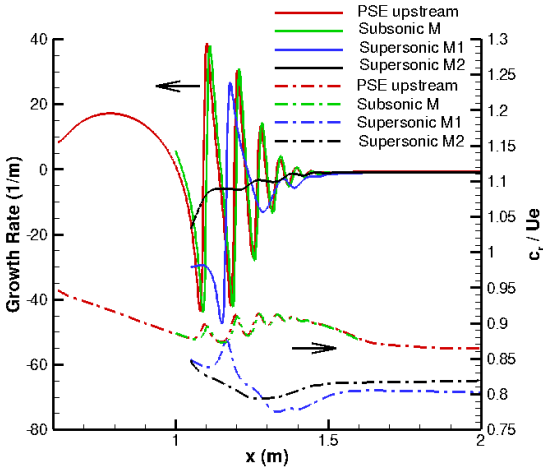

Figure 8. Linear PSE computed disturbance growth rate and phase speed for $f = 500\ kHz$ under $T_w = 500\ K$ wall condition via four different initial starting conditions.

The emergence of unstable supersonic modes as shown above is closely related to the synchronous point of subsonic (S) and supersonic (F) branches of instability modes and deserves more studies. Figure 9 compares the LST predicted eigenmode structures for these two modes at the synchronous point of $x = 0.834\ m$ for the cold wall case shown in Fig. 7. The subsonic and supersonic modes show a single and double outer-peak structure near the critical layer (around $y/l = 5$) for temperature disturbances, respectively. The supersonic mode also introduces an additional outer peak in streamwise velocity disturbances. Due to wall cooling, the inner temperature peak surpasses that of the outer peak for the subsonic mode at this location. In contrast, the supersonic mode exhibits two peaks near the critical layer for temperature disturbances and they are substantially larger than the inner peak near the wall. Interestingly, the corresponding pressure disturbance does not show additional peak near the critical layer, indicating the nonacoustic nature of this mode. The emergence of the supersonic mode can be further realized in the linear PSE results, which incorporate the nonparallel effects due to the boundary-layer growth and have been shown to agree with DNS across the speed regimes and instability mechanisms. In a realistic nonparallel boundary layer, the effective (total) nonparallel wave number is defined by

$$\alpha_{eff} = \alpha - i\,\frac{1}{\phi}\frac{\partial \phi}{\partial x}$$

for any arbitrary disturbance ϕ with a PSE normalized wave number α. The above equation indicates that both phase speed and growth rate vary along the wall-normal direction and with different flow variables. Figure 10 (a) plots the disturbance growth rates measured by three different quantities (wall pressure, kinetic energy and temperature) for the same case shown in Fig. 6. All growth rates agree well in the second-mode region but differ quite a bit as soon as the inception of the unstable supersonic modes, indicating strong nonparallel behavior of the supersonic modes The wall pressure growth rate is the largest among all three. Kinks in maximum temperature growth rates are a direct outcome of eigenfunction peak switching. Four locations indicated in Fig. 10 (a) are selected for further comparisons: P1) peak second-mode location, P2) upper branch second-mode neutral point, P3) first minimum supersonic growth, and P4) first supersonic maximum growth location. The phase speed and growth rates shown in Figs. 10 are calculated based on the temperature disturbance. As shown in Fig. 10 (b), the double outer-peak temperature perturbation structure similar to that shown in Fig. 9 (b) begins to form from location P2 on, and becomes distinct at location P3 near the first minimum supersonic growth rate spike. The formation of the double outer-peak supersonic mode structure is accompanied by the presence of supersonic phase speed below the threshold $1 - 1/M_e$ value across the boundary layer as shown in Fig. 10 (c). In between P1 and P2, the dip in phase speed near the critical layer (around $y/l = 6.5$ at P1) first passes the threshold value around $x = 0.9\ m$, where the synchronization of the acoustic and instability modes allows the supersonic mode to emerge naturally in the nonparallel boundary layer. This nonparallel location of the synchronous point is further downstream of what is predicted by the LST, as expected. Nonparallel growth rates shown in Fig. 10 (d) shows substantial variation across the boundary layer. However, except for P3, growth rate is

rather uniform near the critical layer of $y/l = 5$. It is also evident from Fig. 10 (d) that the oscillatory growth rate spikes starting from the onset of unstable supersonic mode are mainly due to the presence of the double-peak supersonic mode structure and strong growth rate variations in that vicinity of the boundary layer.

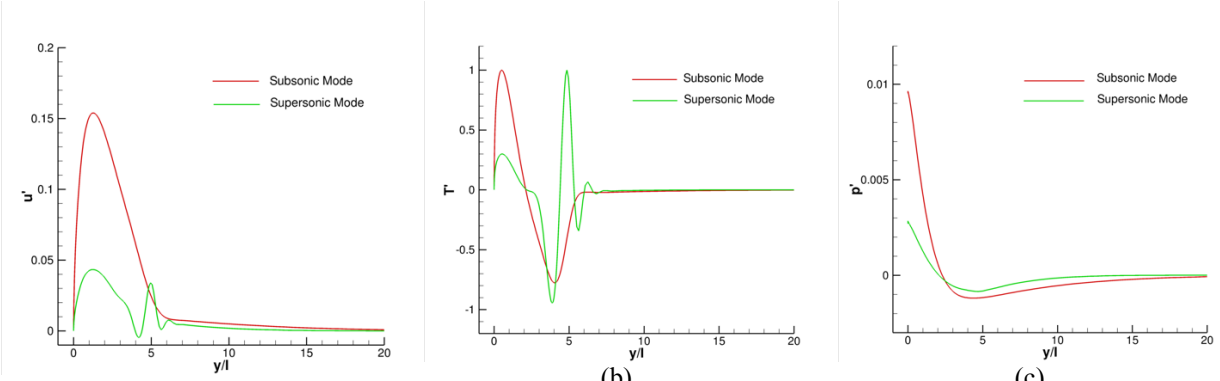

Figure 9. LST predicted eigenmode structure at the synchronous point at $x = 0.834$ for $T_w = 500K$ depicted in Fig. 7 with wall-normal coordinates normalized by the boundary-layer length scale l: (a) streamwise velocity disturbance (b) temperature disturbance (c) pressure disturbance.

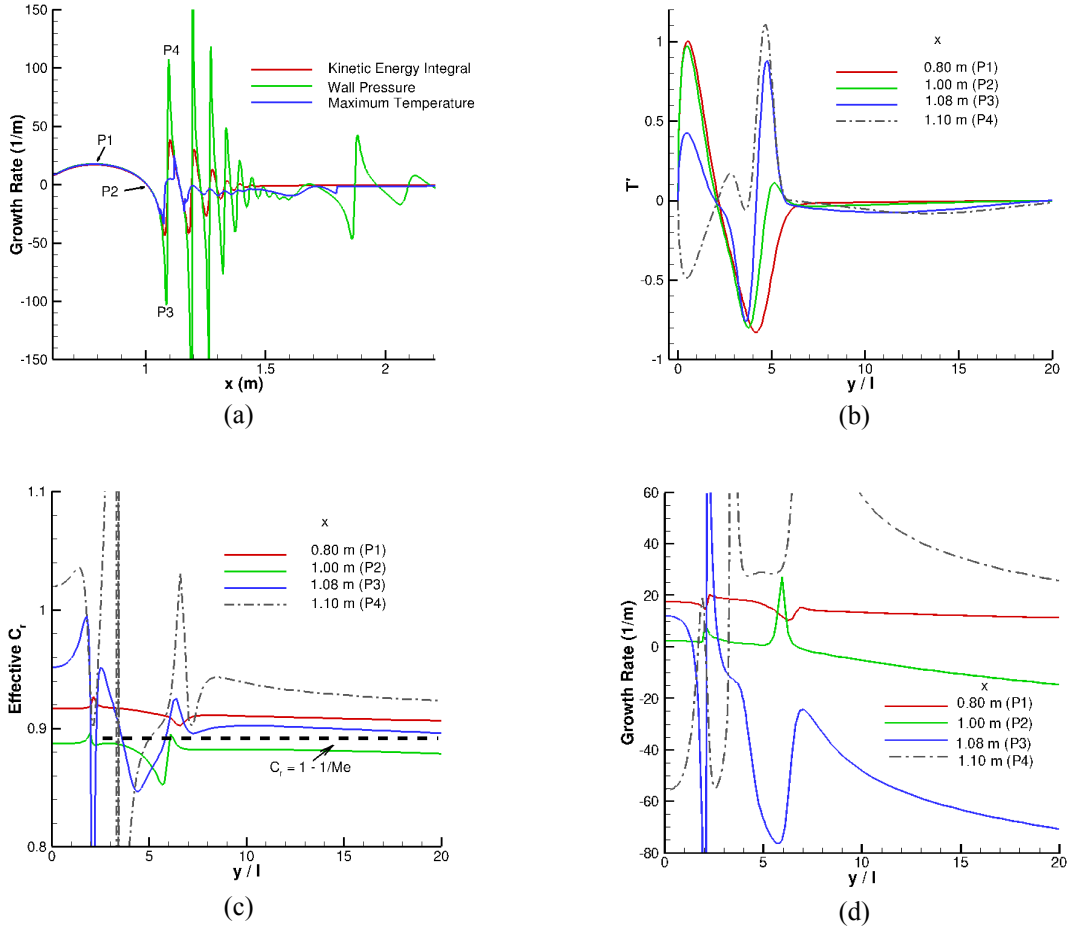

Figure 10. Nonparallel phase speed, growth rates and temperature disturbances predicted by LPSE for the $T_w = 500$ case: (a) three different growth rates versus x, (b) temperature disturbance versus y/l, (c) phase speed versus y/l, and (d) growth rate versus y/l.

The supersonic mode structure can be visualized in Fig. 11 where the PSE predicted pressure perturbation contours are plotted in the computational domain. In the region where the supersonic mode begins to quickly grow and decay (around $x = 1.1$), an acoustic wavelike structure begins to radiate disturbances away from the wall with a phase speed that is lower than the acoustic mode. These radiated waves continue to travel downstream at a small angle (around 2.5°) with respect to the wall, different from the Mach angle at a post-shock Mach number of 9.03. Further research is needed to determine the relation of the supersonic modal structure radiating angle with the Mach wave direction. Similar structures have also been observed from the DNS results for the thermochemical nonequilibrium case [14]. The radiated pressure disturbance layer is certainly not of acoustic nature because it propagates at a different phase speed and does not radiate into the freestream with a Mach angle. Close inspections of the disturbance structure evolution around $x = 0.9 - 1.1$m show that the supersonic-mode pressure pulses are a natural response of the double-peak temperature disturbances due to the inception of the supersonic modes. This double-peak temperature perturbation forms first around $x = 1.0$ m. Further downstream, a growing double-peak temperature disturbance produces pressure pulses and they start to travel away from the wall together as the supersonic mode travels downstream with a phase speed close to the acoustic wave speed.

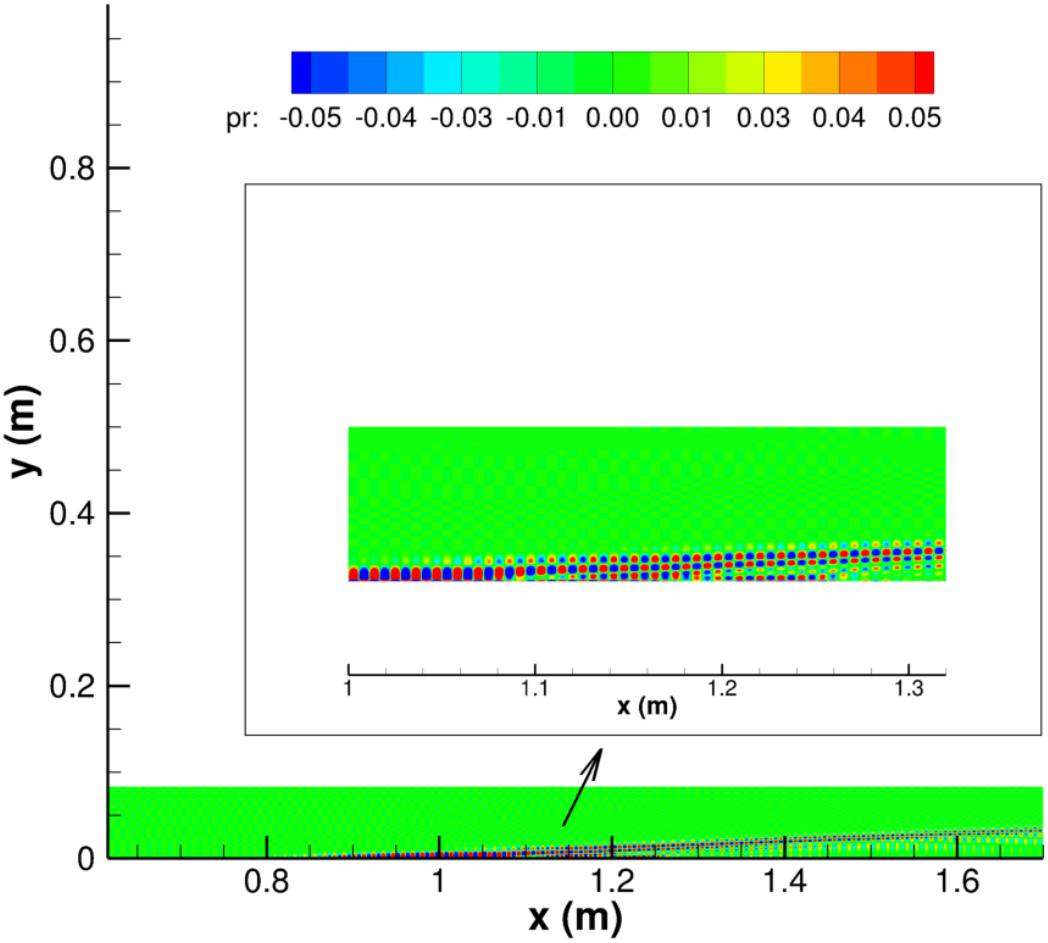

Figure 11. Pressure disturbance structure of supersonic modes computed by linear PSE for $f = 500\ kHz$ under a cold ($T_w = 500\ K$) wall temperature condition.

B. Variation of Supersonic Modes with Mach Numbers under High-Enthalpy Wind Tunnel Conditions

After discussing the onset of unstable supersonic modes due to wall cooling under a high temperature hypersonic condition, questions remain as to whether under more realistic high-enthalpy wind tunnel conditions they would emerge naturally after the second-mode peak growth location or not. For cases studied in this section, freestream conditions are changed to be at typical high-enthalpy wind tunnel running conditions. Using the CUBRC LENS tunnel's operating conditions [25] as a reference, freestream conditions are fixed at Mach 10 with a stagnation temperature and pressure of 12,000 $°R$ and 20,000 psia, respectively. Corresponding static temperature is 571.5 $°R$ (317.5 K) and static pressure is 0.471 psia (3246.5 N/m^2). The computed post-shock Mach number, temperature, and static pressure are 8.77, 387.27 K, and 1.467 psia ($1.012 \times 10^4\ N/m^2$) for a sharp-tip 5° half-angle cone, respectively. Both adiabatic wall and a wall temperature of 500 K in thermochemical equilibrium are computed using the boundary-layer code for comparison. At this lower boundary-layer edge temperature, chemical reactions are not as significant as those investigated in Section A above. Under these conditions, the synchronous location and the LST computed growth rates and phase speeds at the same $f = 500\ kHz$ are shown in Fig. 12 (a). The results are similar to that shown in Fig. 7 under a higher boundary-layer edge temperature except that the predicted synchronous point ($x = 0.9\ m$) is quite close to the peak second mode growth rate location at this frequency. This proximity apparently enhances the unstable supersonic mode downstream of the upper-branch neutral location as shown in Fig. 12 (b). When compared with the results shown in Fig. 6 (a), supersonic modes under this high-enthalpy wind tunnel condition are more unstable in terms of either overall maximum growth rate or number of growing spikes downstream. On the other hand, the predicted phase speed is in a slightly higher range for the current case with only a small portion falling in the supersonic-mode range.

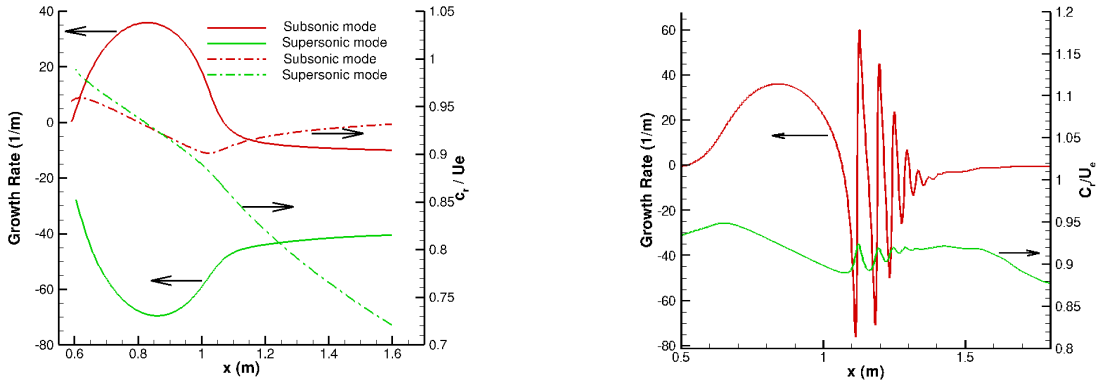

(a) (b)

Figure 12. Unstable supersonic modes at $500kHz$ for a Mach 10 cone under wind tunnel conditions and $T_w = 500K$: (a) LST modes and synchronous location, and (b) LPSE predicted growth rates and phase speed.

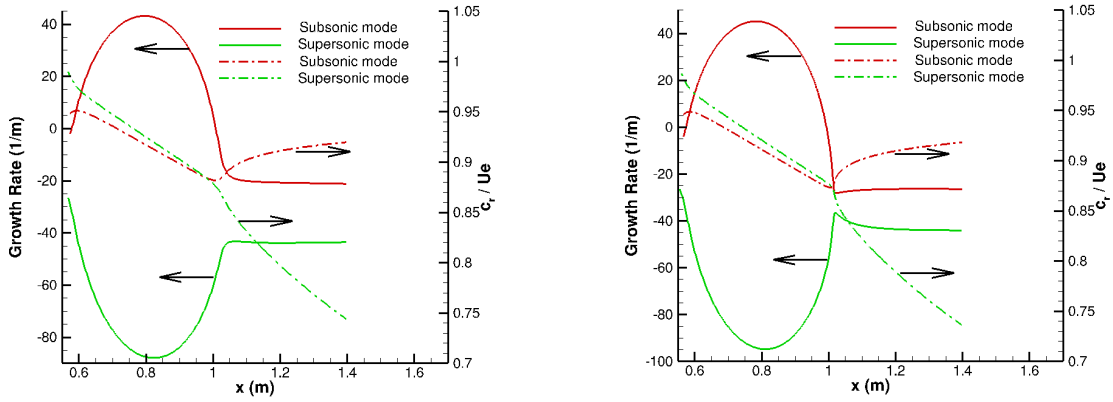

(a) (b)

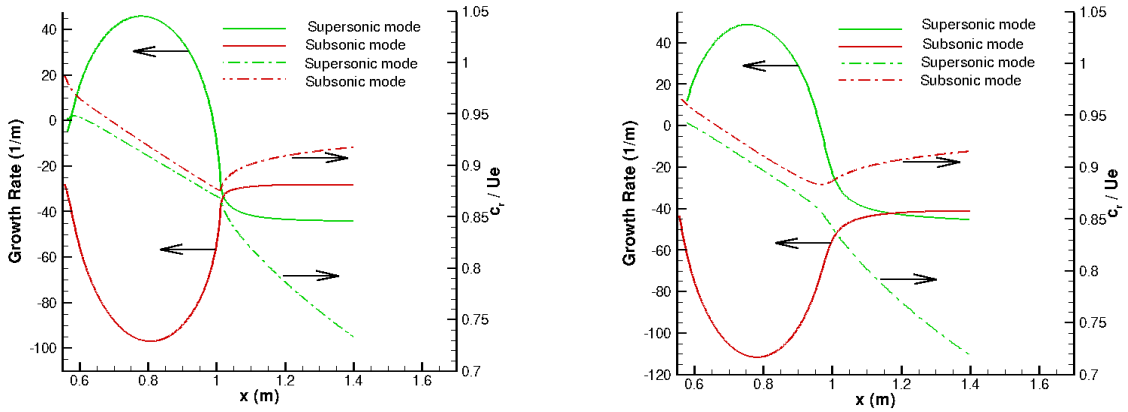

Figure 13. LST predicted variation of synchronous location and dominate subsonic modes with respect to boundary-layer edge Mach number for $T_w = 500K$ and $f = 500kHz$: (a) Mach 7.33, (b) Mach 6.94, (c) Mach 6.83, and (d) Mach 6.17.

For cases discussed so far, the location of the synchronous point appears to be always farther upstream than the location where supersonic modes show their typical spiky growth rate patterns. In fact, for all cases investigated in this study, the onset of unstable supersonic modes correlates well with the location where the nonparallel (PSE) phase speed is in sync with the threshold value of $1 - 1/M_e$ (or more precisely, the phase-speed dip, near the critical layer moves below this threshold), but not with the LST predicted synchronous location. Nonetheless, a synchronous location beyond the second-mode peak serves as an indicator of the existence of supersonic modes. To understand how unstable supersonic modes are related to the Mach number, the same configuration is repeated for several boundary-layer edge Mach numbers by fixing the edge temperature and pressure but varying the streamwise velocity values. This results in a series of edge Mach numbers and the corresponding variation of synchronous locations as shown in Fig. 13. For a Mach 10 flow past a 5° half-angle cone, the boundary-layer edge Mach numbers of 6.17-7.33 as shown correspond to varied high-enthalpy wind tunnel Mach numbers and stagnation conditions. Two major conclusions can be drawn from the results depicted in Fig. 13. Firstly, the synchronous location continues to move downstream when the Mach number is decreased until a value of 6.94. Further decreasing the Mach number, the synchronous point vanishes and the subsonic (S mode) and supersonic (F mode) branches do not intersect at all at this frequency. The two branches also move further apart as the Mach number decreases. Secondly, the dominant (more unstable) branch switches from subsonic (S mode) to supersonic (F mode) when the Mach number is below 6.94. The reason for this switch has roots in its receptivity mechanism with the associated acoustic modes. However, the switch only exists under cooled wall conditions because the dominant branch remains subsonic for the same boundary-layer edge Mach number of 6.17 but with adiabatic wall conditions (see Fig. 14). Even without the synchronization, supersonic modes still appear for the lower Mach number cases (i.e., Figs. 13(c) and 13(d)) because the dominant branch changes from subsonic to supersonic downstream of the upper branch neutral location. This is confirmed in the PSE predicted growth rate and phase speed plot depicted in Fig. 14. As shown, downstream of the upper branch neutral location, supersonic modes appear but they all fall under the stable regime. For comparison, results under the same boundary-layer edge conditions but with an adiabatic wall are also shown in the figure for comparison. As mentioned above, the dominant mode remains subsonic throughout the second-mode unstable region. It should be noted that the reason for all stable supersonic modes under lower Mach numbers is mainly due to the synchronization of the phase speed to the threshold value and takes place in the stable second-mode region, not because of the lack of the two-branch synchronization as in the higher Mach number cases.

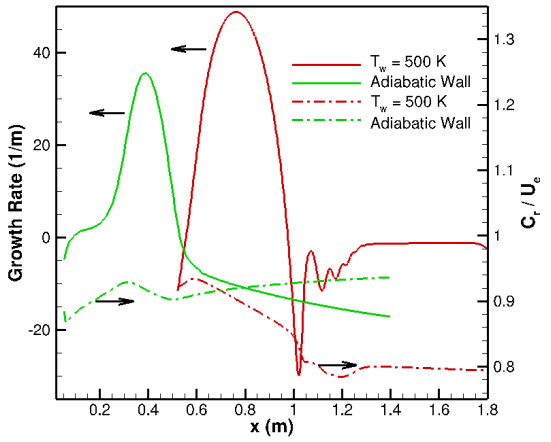

Figure 14. Linear PSE computed disturbance growth rate and phase speed for $f = 500\ kHz$ under two wall conditions for an edge Mach number of 6.17.

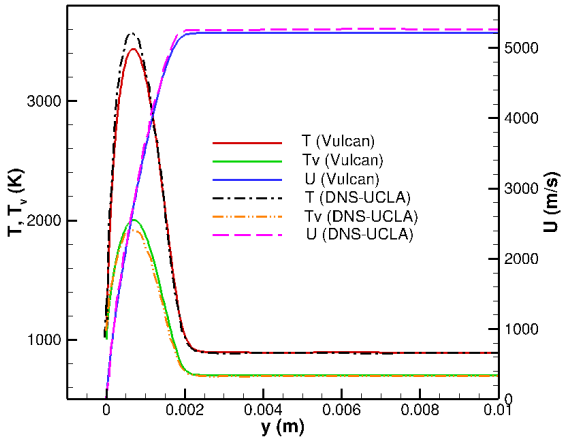

Figure 15. Comparison of mean velocity and two temperatures at $x = 0.4\ m$ with the UCLA results (from Ref. [14]) for the Mach 10 flow over a 5° half-angle blunt cone.

C. Thermochemical nonequilibrium Supersonic Modes Compared with DNS

To assess the thermochemical nonequilibrium effects on supersonic modes, the same Mach 10 cone cases investigated by the UCLA group using DNS [14] are studied using linear PSE here. The freestream temperature and pressure for this Mach 10 flow over a 5° half-angle cone are 700 K and 4000 N/m^2, respectively. The higher static temperature than the canonical cases in Section III.B implies a much higher enthalpy and stronger chemical reactions for this case. Wall temperature was set to be 1000 K in their studies. The mean flow was computed by using the VULCAN code as described earlier using the Park chemistry model [24] (same as in [14]) and a nose radius of 1 mm. The computed streamwise velocity and two temperatures at $x = 0.4\ m$ are compared with the mean solutions from Ref. [14] in Fig.15. There is a slight mismatch in the boundary-layer edge velocity, perhaps due to the difference in shock capturing (VULCAN) and shock fitting (Ref. [14]). Aside from that, substantial discrepancies exist in peak temperatures and small differences in boundary- layer thickness, probably due to differences in boundary-layer edge conditions. Stability results for a disturbance frequency of 700 kHz predicted by linear PSE are compared to that from DNS in Fig. 16 for both growth rates and phase speed. Here the effective nonparallel growth rates and phase speed are measured by the wall pressure disturbance, as was done in the DNS results. PSE results obtained by using the Dunn & Kang model [21] are also shown in the figure for comparison. PSE results for both models, even though exhibiting similar supersonic mode traces, do not agree with DNS. This is not surprising given the visible differences in the mean flow shown in Fig. 15. In general, the current results show more stabilizing supersonic modes after their inception. The supersonic modes in this case apparently track the subsonic phase speed beyond the synchronous location, which is similar to what is recorded in the DNS [14]. Strictly speaking, only a small portion of this mode is supersonic (for $0.4\ m < x < 0.6\ m$). A separate computation using the boundary-layer mean flow code in thermochemical equilibrium produces a more unstable supersonic mode growth at this frequency. More future work is needed to iron out these discrepancies.

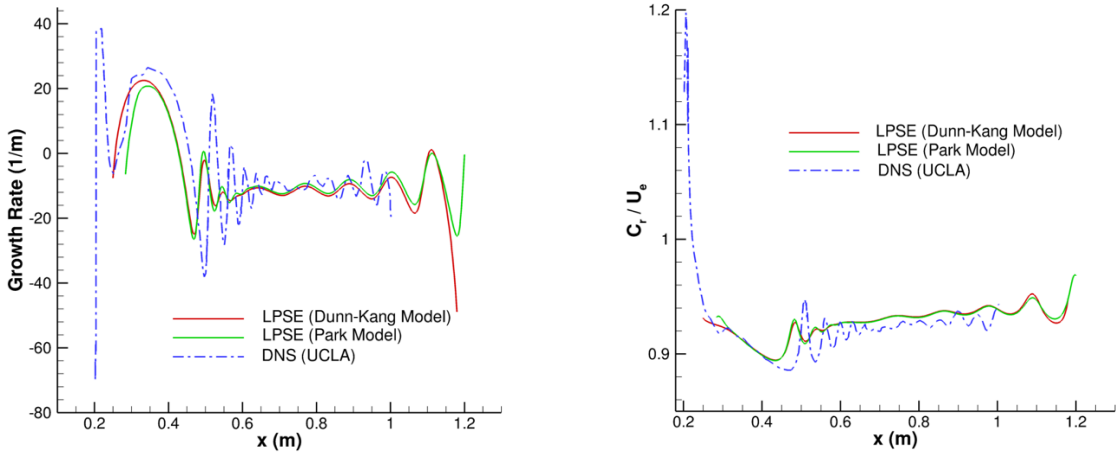

Figure 16. Comparison of linear PSE predicted disturbance growth rates for thermochemical nonequilibrium (TNE) using two different chemistry models at $f = 700kHz$ with results from DNS [14]: (a) growth rates and (b) phase speed.

D. Effects of Wall Cooling on Fixed-Frequency Supersonic Modes

To understand how the growth rate of supersonic modes is influenced by the wall cooling, the results shown in Section III.C are extended to various wall temperatures using the boundary-layer code for thermal equilibrium flows with finite-rate chemistry. The corresponding adiabatic wall temperature for this case, as computed by the boundary-layer code, varies in a range with an average around 7000K. The wall temperature studied varies from 100-1000K, corresponding to a T_w/T_{adw} ratio of about 0.014-0.14. Figures 17 and 18 show the PSE computed growth rates and phase speed, respectively. Note that results for some temperatures are not shown in Fig. 17 for clarity. Stronger wall cooling appears to first increase and then decrease the overall peak of the supersonic-mode growth rates. It is interesting to note that the supersonic-mode phase speed falls mostly in the subsonic range when the wall temperature is high (400-1000 K). The phase speed continues to decrease as the wall temperature is decreased. For the two coldest wall cases (100 and 200 K), the phase speeds are entirely in the supersonic range (smaller than 0.89). The integrated overall growth (N factor) at a disturbance frequency of 500 kHz is shown in Fig. 19 for various wall temperatures. The peak N value due to the second mode is increasing as wall temperature is reduced owing to the destabilizing effect of wall cooling on the second mode. On the other hand, despite the large variation of oscillatory growth rate values, the overall bumpy disturbance amplitude growth and decay in the supersonic mode region for various wall temperatures appears to be insensitive to wall temperature. The presence of supersonic modes acts to slow down the overall disturbance amplitude decay. It remains to be seen if this would affect the nonlinear modal interaction that would eventually lead to transition. It should be cautioned that the overall effects on transition of wall cooling should be evaluated by the N-factor envelopes, not by the N-factor for a single frequency done here. Results shown here are meant to be an initial assessment of wall-cooling effects on a single disturbance mode.

For thermochemical nonequilibrium boundary layers, wall cooling appears to have a more pronounced effect on supersonic modes, as is evident from Fig. 20 for a disturbance frequency of $500kHz$ and four different wall temperatures ranging from 100K to 1000K. At this frequency, wall cooling appears to be strongly destabilizing for supersonic modes. When the wall temperature is further cooled to 300K or lower from the conditions shown in the comparisons with DNS in Fig. 16, the peak supersonic mode growth rate increases first and then decreases again for the lowest wall temperature, all under the assumption of thermochemical nonequilibrium. The trend is consistent with the findings for thermal equilibrium flows shown in Fig. 17. The phase speed variation for all four wall temperatures agree qualitatively with those shown in Fig. 18 for flows under the thermal equilibrium conditions, except that the lowest wall temperatures do not lower the phase speed as significantly. The overall disturbance growth in terms of N factor depicted in Fig. 21 (a) takes a similar trend and is close to that predicted for thermal equilibrium flows. Furthermore, the synchronization of subsonic and supersonic modes for all four thermal nonequilibrium cases appears to be very similar to the results shown in Fig. 12(a). For example, the synchronous location for the $T_w = 200K$ case

shown in Fig. 21 (a) was found to be at $x = 0.96\ m$, substantially upstream of the upper-branch neutral location and the onset of unstable supersonic modes. Formation of the double outer-peak temperature disturbance structure around the upper-branch neutral location (shown in Fig. 21 (b) at four representative streamwise locations) as well as the pressure disturbance radiation (shown in Fig. 22 for $T_w = 200K$), similar to that observed for thermal equilibrium boundary layers in Section III.A (see Fig. 11), are also evident for all three wall temperatures with thermochemical nonequilibrium. Such results suggest that the stability characteristics observed in Sections III.A and III.B under the assumption of thermal equilibrium (using the boundary-layer mean flow) would be in a high likelihood to be valid for thermochemical nonequilibrium hypersonic boundary layers as well.

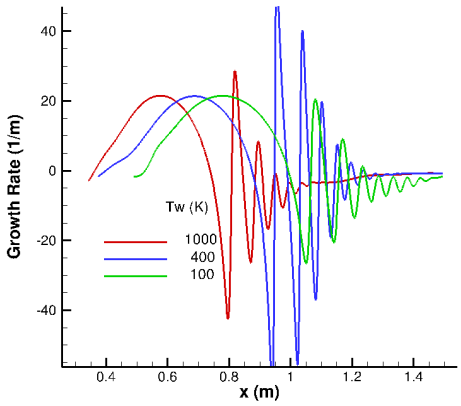

Figure 17. Effects of wall temperature on supersonic mode growth rates ($f = 500kHz$) with mean flows computed by assuming thermal equilibrium using the boundary-layer code.

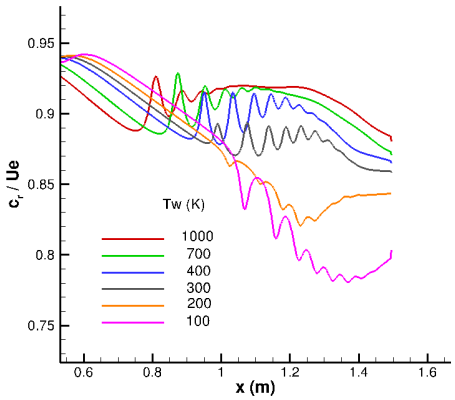

Figure 18. Phase speed variation with wall temperature for $f = 500kHz$ with mean flows computed by assuming thermal equilibrium using the boundary-layer code.

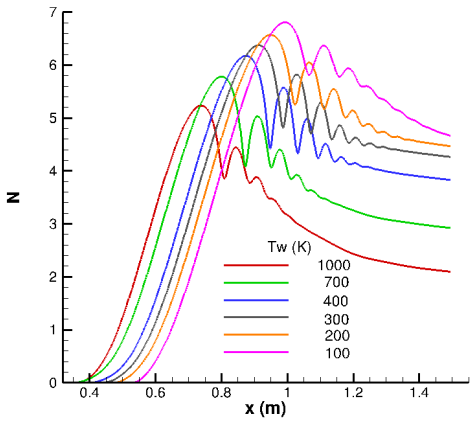

Figure 19. N factors for disturbances with $f = 500kHz$ with various wall temperature, showing effects of wall cooling on supersonic mode growth in thermal equilibrium.

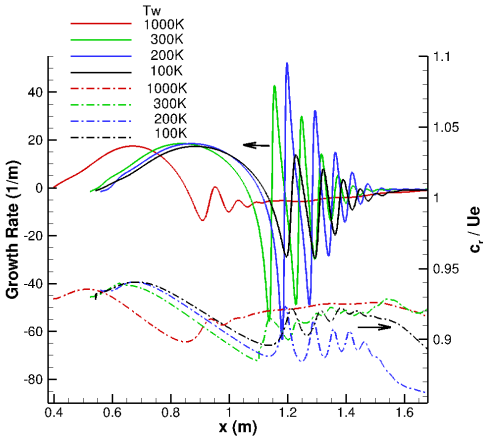

Figure 20. Disturbance growth rate and phase speed for $f = 500kHz$ and four different wall temperatures with mean flows computed by assuming thermochemical nonequilibrium using the Vulcan code [19].

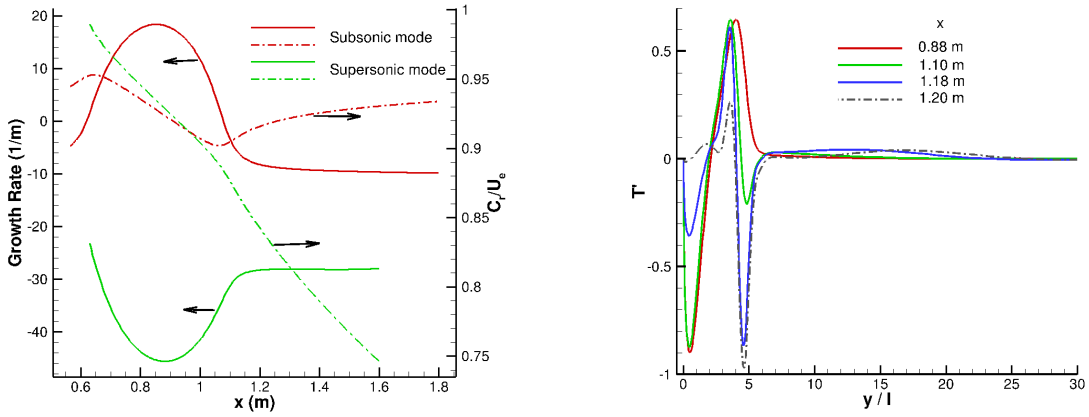

(a) (b)

Figure 21. Evolution of supersonic modes with $T_w = 200K$ for mean flows in thermochemical nonequilibrium: (a) LST predicted synchronization of subsonic and supersonic modes and (b) PSE predicted temperature disturbance shapefunctions at four representative locations (normalization length scale $l = 3.94 \times 10^{-4}\ m$).

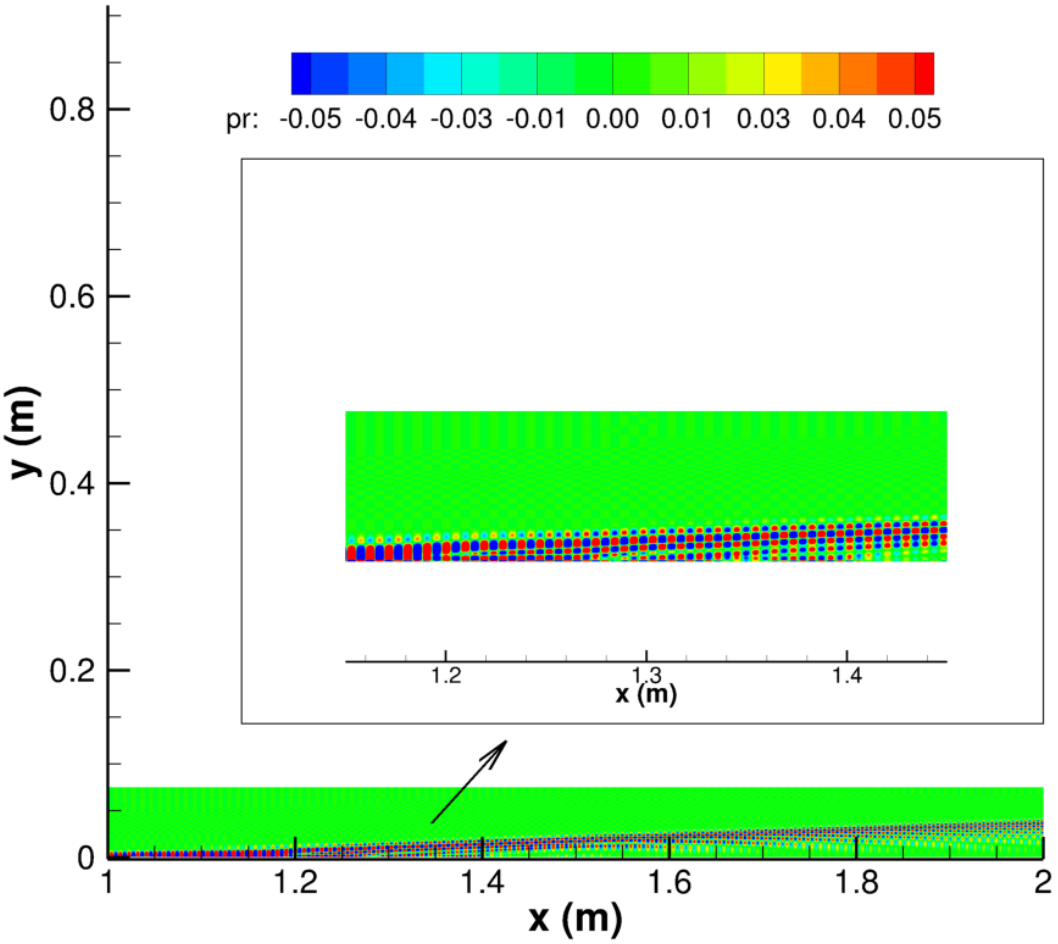

Figure 22. Pressure disturbance structure of supersonic modes computed by linear PSE for $f = 500\ kHz$ under a cold ($T_w = 200\ K$) wall temperature condition for meanflows in thermochemical nonequilibrium.

IV. Concluding Remarks

The onset of supersonic modes and effects of wall cooling on their disturbance growth have been studied for hypersonic flow over a 5° half-angle cone operating at both high static temperature and nominal high-enthalpy wind tunnel conditions. Both LST and linear PSE as implemented in the LASTRAC software are used to study how wall cooling leads to the onset of oscillatory growth/decay of supersonic modes beyond the second mode peak location. It was found that wall cooling thins the boundary layer and moves the generalized inflectional point closer to the wall where the convecting speed is smaller. When this convecting speed is smaller than the threshold value of the supersonic mode phase speed, $1 - 1/M_e$, unstable supersonic modes emerge naturally. The phase speeds of these unstable supersonic modes as they travel downstream could be either subsonic or supersonic, depending on the wall temperature and boundary-layer edge Mach number. A colder wall results in lower unstable supersonic mode phase speeds. Based on the linear PSE results obtained from mean flows computed by a reacting boundary-layer code with thermochemical equilibrium assumptions, unstable and spiky unstable supersonic modes are closely related to the synchronization of the subsonic (S) mode and supersonic (F) mode branches. A synchronous point downstream of the peak second-mode location appears to prompt the onset of possibly unstable supersonic modes downstream beyond the upper-branch neutral location. Similar phenomena were also observed consistently for boundary layers under thermochemical nonequilibrium, qualitatively similar to the recent DNS study in Ref. [14], despite the fact that mean flows computed in the present study differ from their shock-fitting results.

In a nonparallel boundary layer, the emergence of supersonic modes begins when a portion of the boundary layer has an instability wave phase speed that is lower than the theoretical threshold of $1 - 1/M_e$. From that location on, a double outer-peak temperature disturbance structure forms. The double-peak temperature perturbations resemble the eigenfunctions of the supersonic (F) mode predicted by the quasiparallel linear stability theory. This double outer-peak temperature disturbance, which characterizes the existence of supersonic modes, then triggers a pressure disturbance layer that radiates into the freestream with a phase speed that is either higher or lower than the acoustic wave phase speed. According to the present linear PSE results, contrary to what was stated in the literature, supersonic-mode pressure disturbance structure radiated into the freestream is nonacoustic in nature and the formation of unstable supersonic modes is mainly associated with the synchronization of phase speed between the instability and acoustic waves in a nonparallel boundary layer, not due to nonlinear modal interaction as speculated in Ref. [14]. In this regard, the spiky growth rate variation of supersonic modes observed in hypersonic boundary layers can be viewed as an outcome of nonparallel effects due to the synchronization with the acoustic mode when the wall is sufficiently cooled. Preliminary results from single frequency comparisons indicate that the supersonic modes do not lead to stronger overall disturbance growth, but rather, prevent disturbance from decaying fast beyond the upper branch neutral location of the second mode. This phenomena is likely to have strong implication in nonlinear modal interactions that would cause transition in hypersonic boundary layers with a cold wall.

Acknowledgments

The funding for this research has been provided by the Hypersonics Technology Project under the Aeronautics Mission Directorate. The authors would like to acknowledge the help from Rob Baurle of NASA LaRC in generating nonequilibrium meanflows using the Vulcan code.

References

[1] Saric,W.S., Reshotko,E., and Arnal,D., "Hypersonic Laminar-Turbulent Transition," *AGARD Advisory Report*,Vol.2,1998, pp. 2–2. URL https://www.sto.nato.int/publications/AGARD/AGARD-AR-319-02/03chap02.pdf.

[2] Kimmel, R., "Aspects of Hypersonic Boundary Layer Transition Control," AIAA Paper 2003-772, 2003.

[3] Li, F., Choudhari, M., Chang, C.-L., Kimmel, R., Adamczak, D., and Smith, M., "Hypersonic Transition Analysis for HiFiRe Experiments," RTO AVT-200 RSM-030 Specialists Meeting on Hypersonic Laminar-Turbulent Transition, San Diego, CA, April, 2012

[4] Tufts, M. W. and Kimmel, R. L., "Stability Equation Based Transition Prediction," AIAA Paper 2018-0031, 2018.

[5] Mack, L. M., "Boundary-Layer Linear Stability Theory," Tech. rep., California Institute of Technology Jet Propulsion Laboratory, 1984. URL http://www.dtic.mil/docs/citations/ADP004046.

[6] Stetson, K., Kimmel, R., Donaldson, J., and Siler, L., "A Comparison of Planar and Conical Boundary Layer Stability and Transition at a Mach Number of 8," AIAA Paper 1991-1639, 1991.

[7] Malik, M. R., "Prediction and Control of Transition in Supersonic and Hypersonic Boundary Layers," *AIAA Journal*, Vol.27, No. 11, 1989, pp. 1487–1493. doi:10.2514/3.10292, URL http://arc.aiaa.org/doi/10.2514/3.10292.

[8] Chang, C.-L., Vinh, H., and Malik, M., "Hypersonic Boundary-Layer Stability with Chemical Reactions Using PSE,"

AIAA Paper 1997-2012, 1997. doi:10.2514/6.1997-2012, URL http://arc.aiaa.org/doi/10.2514/6.1997-201.

[9] Johnson, H., and Candler, G., "PSE Analysis of Reacting Hypersonic Boundary Layer Transition," AIAA Paper 1999-3793, 1999.

[10] Malik, M. R., "Hypersonic Flight Transition Data Analysis Using Parabolized Stability Equations with Chemistry Effects," *Journal of Spacecraft and Rockets*, Vol. 40, No. 3, 2003, pp. 332–344. doi:10.2514/2.3968, URL http://arc.aiaa.org/doi/10.2514/2.3968.

[11] Johnson, H., and Candler, G., "Analysis of Laminar-Turbulent Transition in Hypersonic Flight Using PSE-Chem," AIAA Paper 2006-3057, 2006.

[12] Chuvakhov, P. and Federov, A., "Spontaneous Radiation of Sound by Instability of a Highly Cooled Hypersonic Boundary Layer," *J. Fluid Mech*. Vol. 805, pp. 188-206, 2016.

[13] Edward, L. and Tumin, A., "Real Gas Effects on Receptivity to Kinetic Fluctuations: I. Mean Flow Effects," AIAA Paper 2017-0070, 2017.

[14] Knisely, C. P. and Zhong, X., "Significant Supersonic Modes and the Wall Temperature Effect in Hypersonic Boundary Layers," *AIAA J*. Vol. 57, No. 4, pp. 1552-1566, April 2019.

[15] Kline, H., Chang, C.-L., and Li, F., "Hypersonic Chemically Reacting Boundary-Layer Stability Using LASTRAC," AIAA Paper 2018-3699, 2018.

[16] Kline, H., Chang, C.-L., and Li, F., "Boundary Layer Stability and Transition in a Chemically Reacting Martian Atmosphere Using LASTRAC," AIAA Paper 2018-5206, 2018.

[17] Chang, C.-L., "Langley Stability and Transition Analysis Code (LASTRAC) Version 1.2 User Manual," *NASA TM2004-213233*. URL https://ntrs.nasa.gov/search.jsp?R=20040082550.

[18] Blottner, F. G., Johnson, M. and Ellis, M., "Chemically Reacting Viscous Flow Program for Multi-Component Gas Mixtures," Report No. SC-RR-70-754. Sandia National Labs, Albuquerque, NM. 1971.

[19] "VULCAN," http://vulcan- cfd.larc.nasa.gov/, 2016 (last accessed 02/07/2018).

[20] White, J.A. and Morrison, J. H., "Pseudo-Temporal Multi-Grid Relaxation Scheme for Solving the Parabolized Navier-Stokes Equations," AIAA Paper 99-3360, 1999.

[21] Dunn, M. G., and Kang, S., "Theoretical and Experimental Studies of Reentry Plasmas," NASACR-2232, NASA, April1973. URL https://ntrs.nasa.gov/search.jsp?R=19730013358.

[22] Gupta, R. N., Yos, J. M., Thompson, R. A., and Lee, K.-P., "A Review of Reaction Rates and Thermodynamic and Transport Properties for an 11-Species Air Model for Chemical and Thermal Non-equilibrium Calculations to 30000 K," NASA RP-1232, NASA, 1990. URL https://ntrs.nasa.gov/search.jsp?R=19900017748.

[23] Blottner, F. G., "Viscous Shock Layer at the Stagnation Point with Nonequilibrium Air Chemistry," *AIAA Journal*, Vol.7, No.12, 1969, pp. 2281–2288. doi:10.2514/3.5528.

[24] Park, C., and Yoon, S., "Fully Coupled Implicit Method for Thermochemical Nonequilibrium Air at Suborbital Flight Speeds," *Journal of Spacecraft and Rockets*, Vol. 28, No. 1, 1991, pp. 31–39.

[25] "Large Energy National Shock Tunnel (LENS)," Calspan-UP Research Center, P. O. Box 400, Buffalo, NY 14225, May 25, 1995.